JGR Atmospheres

RESEARCH ARTICLE
10.1029/2020JD034513

The Influence of Stratospheric Soot and Sulfate Aerosols on the Northern Hemisphere Wintertime Atmospheric Circulation

Joshua Coupe[1] **and Alan Robock**[1]

[1]Department of Environmental Sciences, Rutgers University, New Brunswick, NJ, USA

Key Points:

- Acceleration of the stratospheric polar vortex (SPV) occurs due to heated stratospheric aerosols in nuclear war and volcanic eruption simulations
- A tropospheric mechanism for acceleration of the SPV is detected in a 150 Tg soot nuclear war scenario
- Winter warming is simulated after the 1963 Agung, 1982 El Chichón, and 1991 Pinatubo volcanic eruptions, when the observed sea surface temperatures, which include an El Niño in each case, are specified

Correspondence to:
J. Coupe,
josh.coupe@rutgers.edu

Citation:
Coupe, J., & Robock, A. (2021). The influence of stratospheric soot and sulfate aerosols on the Northern Hemisphere wintertime atmospheric circulation. *Journal of Geophysical Research: Atmospheres*, *126*, e2020JD034513. https://doi.org/10.1029/2020JD034513

Received 27 DEC 2020
Accepted 24 MAY 2021

Author Contributions:
Conceptualization: Alan Robock
Formal analysis: Joshua Coupe, Alan Robock
Funding acquisition: Alan Robock
Investigation: Joshua Coupe, Alan Robock
Methodology: Alan Robock
Visualization: Joshua Coupe
Writing – original draft: Joshua Coupe
Writing – review & editing: Joshua Coupe, Alan Robock

Abstract The Northern Hemisphere wintertime circulation response to volcanic eruptions has been explored extensively using general circulation models. In observations and some models, the response is characterized by an enhanced stratospheric polar vortex (SPV), a positive mode of the North Atlantic Oscillation (NAO), and warm surface temperatures during the winter over North America and Eurasia. A weak surface air temperature signal in previous studies has led to conflicting conclusions on the robustness of the response. Here, we use simulations with the National Center for Atmospheric Research (NCAR) Whole Atmosphere Community Climate Model (WACCM) of six nuclear war scenarios to present a new perspective on the connection between stratospheric aerosol heating, the SPV, and the surface temperature response. We show that stratospheric aerosol heating by soot is the primary contributor to the SPV response in nuclear war simulations, which is coupled to the troposphere and projects as a positive mode of the NAO at the surface. Winter warming is observed across northern Eurasia, albeit poleward of the response after volcanic eruptions. We compare the results to simulations of volcanic eruptions and find that observed Eurasian warming in the first winter after the 1963 Agung, 1982 El Chichón, and 1991 Pinatubo volcanic eruptions is simulated with the NCAR CAM5 climate model only when tropical sea surface temperatures, including the observed El Niño, are specified along with the volcanic aerosols. This suggests an undiagnosed tropospheric mechanism connecting the tropics and high latitudes, as without specifying sea surface temperatures, internal variability dominates the simulated winter warming response after historical volcanic eruptions.

Plain Language Summary Explosive volcanic eruptions can create sulfur aerosols in the upper atmosphere, which both cool Earth's surface and heat the lower stratosphere. While large heating is well known to affect the atmospheric circulation, favoring a pattern that produces winter surface warming over Eurasia, whether the observed winter warming from eruptions like the 1991 Pinatubo was caused by those eruptions has been questioned. We use nuclear war simulations to show that large heating of the upper atmosphere by smoke would produce this response. Finally, we find that when there is an El Niño combined with a large volcanic eruption, there is a greater likelihood of winter warming over Eurasia.

1. Introduction

Considerable effort has been devoted to characterizing the forced climate response of explosive volcanic eruptions. In particular, the significance of the "winter warming" of continental areas in the Northern Hemisphere following the June 1991 Mount Pinatubo volcanic eruption has been extensively explored and debated. The observed pattern, featuring above average temperatures across North America and Eurasia (Figure 1a), has been attributed to a forced circulation response (Robock & Mao, 1992) as well as simply internal variability (Polvani et al., 2019). The forced circulation response hypothesis is disputed, largely because the forced surface response in several state-of-the-art climate models does not resemble the observed response. A similar type of forced circulation response has also been studied in the context of solar radiation management schemes to alleviate anthropogenic global warming, which could produce upper atmospheric heating similar to volcanic eruptions; several studies have found a robust circulation and winter warming response associated with this type of stratospheric aerosol injection (Banerjee et al., 2021; Jones et al., 2020).

In simulations of historical volcanic eruptions, two primary mechanisms have been proposed to explain the tendency for a positive mode of the Arctic Oscillation (AO) and a strengthened stratospheric polar vortex

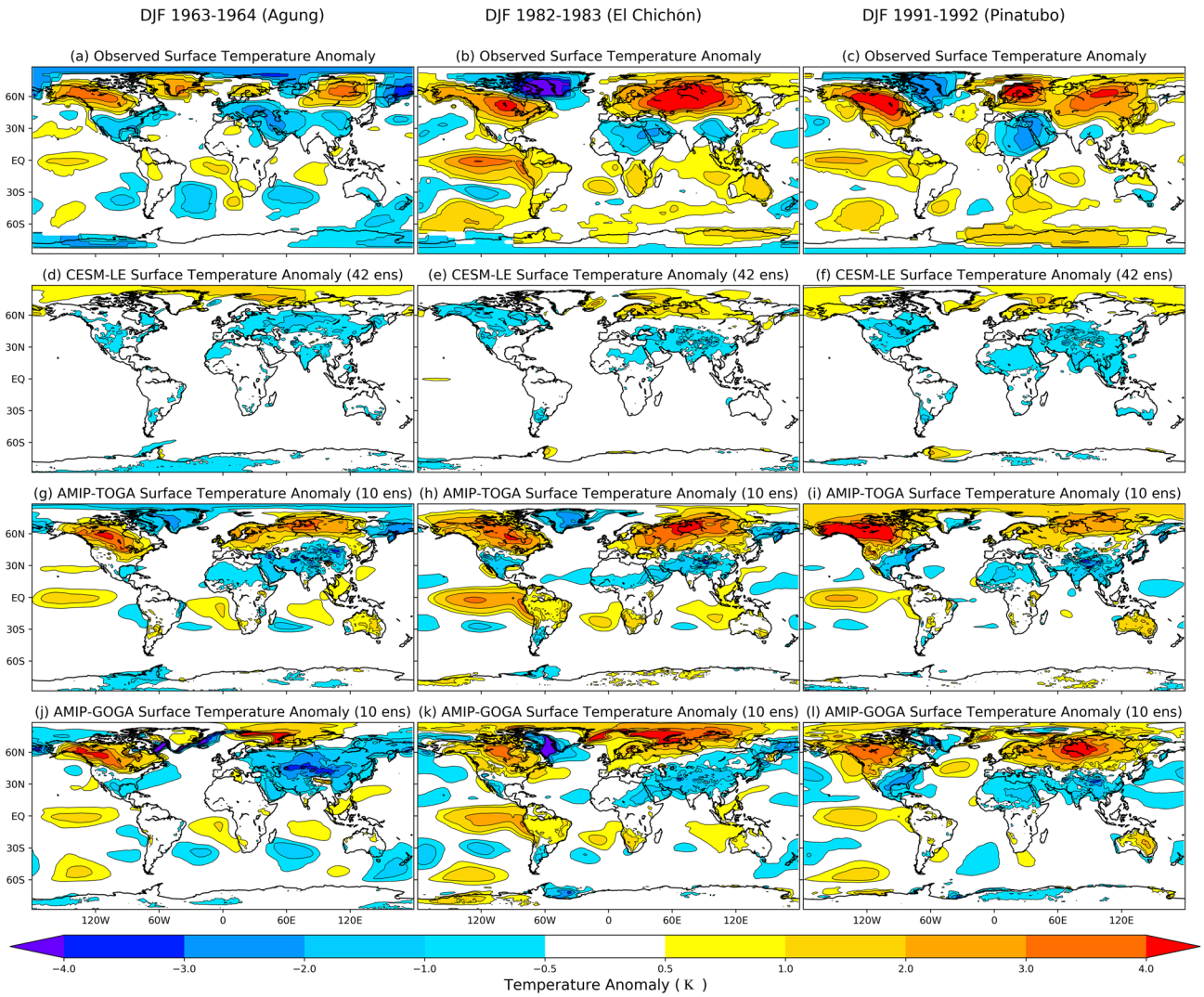

Figure 1. GISS surface temperature analysis (GISTEMP team, 2020) version 4 observed surface temperature anomaly (K) with respect to the previous 5 years during (a) December-January-February (DJF) 1963–1964, (b) DJF 1982–1983 and (c) DJF 1991–1992. Ensemble mean surface temperature anomaly (K) in Community Earth System Model-Large Ensemble (CESM-LE) for the same period (d–f), in Atmospheric Model Intercomparison Project-Tropical Ocean Global Atmosphere (AMIP-TOGA) (g–i), and in AMIP-Global Ocean Global Atmosphere (GOGA) (j–l). DJF 1963–1964, (h) DJF 1982–1983 and (i) DJF 1991–1992.

(SPV). The first is the stratospheric mechanism, first explored by Graf et al. (1993). The stratospheric mechanism was initially described as an acceleration of the Northern Hemisphere SPV during the winter due to the lack of aerosol heating over the pole compared to the midlatitudes and tropics. To achieve thermal wind balance in response to the strong stratospheric temperature (and geopotential height) gradient, a westerly acceleration of the SPV is expected to occur. During winter, strong anomalies in the SPV tend to propagate vertically toward the surface, favoring a positive AO and/or North Atlantic Oscillation (NAO) (e.g., Baldwin & Dunkerton, 2001). However, according to some work, the strongest stratospheric temperature gradient is in the subtropics during the winter, and the need to achieve thermal wind balance produces a direct acceleration of the subtropical jet more so than the polar jet (Bittner et al., 2016a; DallaSanta et al., 2019; Toohey et al., 2014). To explain why the SPV is strengthened beyond what the temperature gradient implies, it has been proposed that the acceleration of the subtropical jet limits the poleward propagation of planetary waves by deflecting them toward the equator, allowing for the SPV to further accelerate (Bittner et al., 2016b; DallaSanta et al., 2019). Thus, the stratospheric mechanism may require an acceleration of the stratospheric subtropical jet and the deflection of poleward propagating planetary waves to explain the enhancement of the polar vortex in model simulations of volcanic eruptions. The strengthening of the SPV

is amplified by a feedback where a stronger SPV reflects planetary waves, limiting disruptions of the vortex and allowing it to remain symmetric about the pole (Stenchikov et al., 2002).

An additional tropospheric mechanism that has received little attention has also been proposed to strengthen the SPV, which then influences the troposphere through coupling. Stenchikov et al. (2002), using the SKYHI model, found that the heating of sulfate aerosols was not necessary to force a positive AO after the eruption of Mt. Pinatubo, in support of this mechanism. The tropospheric mechanism, similar but in the opposite direction of the proposed mechanism for producing a weaker jet stream with anthropogenic global warming, is caused by surface cooling in the subtropics, which results in a decrease in the mean meridional temperature gradient in the winter troposphere between 30°N and 60°N. The reduction in this temperature gradient has been suggested to reduce baroclinicity, and thus also reduces the amplitude of planetary waves in the troposphere as well as the vertical wave activity flux from the troposphere into the stratosphere (DallaSanta et al., 2019; Stenchikov et al., 2002). This reduction in wave activity could limit disruptions to the SPV and is associated with a strong, resilient SPV that is resistant to deceleration or breaking down. This mechanism is less relevant for geoengineering proposals that aim to counter global warming, as they are designed, in some scenarios, to not affect the tropospheric pole-to-equator temperature gradient (e.g., Tilmes et al., 2018).

The evidence for either of these mechanisms in the historical observations has been disputed. It is also difficult to confirm a cause-and-effect relationship for smaller aerosol loading cases without large ensembles, but nuclear war simulations amplify the forced signal and provide clarity for the mechanisms that contribute to the zonal mean wind response. The changes to the stratosphere are amplified such that heating of the surrounding air by the aerosols reaches nearly 100 K due to the absorptive nature of black carbon, as much as 50 times the amount of heating after Pinatubo, which was 2 K according to reanalysis (Polvani et al., 2019). Soot aerosols have an *e*-folding lifetime of more than three times that of volcanic sulfate aerosols because they are lofted to higher altitudes, which also increases the duration of the circulation response (Coupe et al., 2019). Nuclear war simulations are an extreme case compared to tropical volcanic eruptions of the past century and provide an opportunity to amplify stratospheric heating and surface cooling, enhancing the forcing with fewer ensemble members required.

2. Data and Methods

Here, we use model simulations of both volcanic eruptions and nuclear war to explore the impact of stratospheric aerosol injection on atmospheric circulation. Other aspects of climate change in these nuclear war simulations have been previously reported (Coupe et al., 2019, 2021; Toon et al., 2019). We use the Community Earth System Model version 1.3 (CESM), containing coupled atmosphere, ocean, sea ice, and land components. For the atmospheric component, we use the Whole Atmosphere Community Climate Model version 4 (WACCM4), which has a horizontal resolution of 1.9° × 2.5° with 66 vertical layers and a 140 km model top (Marsh et al., 2013) and hereafter, we refer to this model configuration as WACCM4. In addition to stratospheric interactive chemistry, WACCM4 is coupled to the Community Aerosol and Radiation Model for Atmospheres (CARMA), a sectional aerosol model which treats soot aerosols as fractal particles that are allowed to coagulate, altering their optical properties (Bardeen et al., 2008, 2017; Toon et al., 1988). Six nuclear war scenarios are examined, where varying amounts of soot aerosols are injected into the 150–300 hPa layer over different areas, based on the work of Robock et al. (2007) and Toon et al. (2019). The largest United States and Russia nuclear war scenario is simulated as a 150 Tg soot injection over the United States and Russia, beginning on May 15 and lasting for one week. The five other scenarios inject 5, 16, 27.3, 36, and 46.8 Tg of soot over India and Pakistan with the same start date, duration, and altitude. Three ensemble members were conducted for the 5 Tg case to assess the role of internal variability, but the large forced response of most climate variables for simulations with more than 5 Tg of soot makes the need for extensive ensembles unnecessary. A 60-year control climatology is used to calculate anomalies, which is based on the year 2000 and has CO_2 fixed at 370 ppm, which are the same boundary conditions as the nuclear war simulations. Some of the extreme conditions imposed by a large injection of soot into the upper atmosphere are outside of the typical range for the chemistry and physics schemes used in this model, and cannot be tested with observations. This introduces some uncertainty, especially for some of the nonlinear components of the climate system relevant in this analysis, but we have no evidence of erroneous behavior in the results.

To compare with the response after volcanic eruptions, we examine the forced response of the Northern Hemisphere wintertime circulation of historical volcanic eruptions in the CESM Large Ensemble (CESM-LE, Kay et al., 2015), comprising 42 ensembles covering the 1920–2006 period. The Community Atmosphere Model version 5 (CAM5) was used as the prognostic atmospheric component and the Parallel Ocean Program model version 2 (POP2) was used as the prognostic ocean. We examine the winter period, December-January-February (DJF) immediately following the March 1963 Agung, April 1982 El Chichón, and June 1991 Mt. Pinatubo eruptions. All temperature anomalies are calculated with respect to the previous 5 years, following Zambri and Robock (2016). This retains the volcanic signal but may also include some influences from El Niño or La Niña events that occurred in the previous 5 years, if they were simulated by the climate model.

Additionally, we use 10 ensembles designated as the Atmospheric Model Intercomparison Project-Tropical Ocean Global Atmosphere (AMIP-TOGA), which are configured like CESM-LE, except they are specified with historical sea surface temperatures (SSTs) between 28°S and 28°N (Deser et al., 2017; Lehner et al., 2018). Elsewhere, climatological SSTs are imposed. AMIP-TOGA allows us to ascertain the role of historical tropical SSTs on replicating the observed temperature patterns after these three eruptions. In addition to AMIP-TOGA, we utilize 10 ensembles of the Atmospheric Model Intercomparison Project-Global Ocean Global Atmosphere (AMIP-GOGA) simulations, which are run with the same model configuration as AMIP-TOGA, but instead observed SSTs are prescribed globally (Deser et al., 2017; Lehner et al., 2018).

Surface temperature anomalies from the GISS Surface Temperature Analysis version 4 (GISTEMP4) are used to compare the model response with the observed surface temperature response (GISTEMP Team, 2020; Lenssen et al., 2019). GISTEMP4 combines land (GHCN version 4) and ocean (ERSST version 5) observations into a single data set. GISTEMP4 anomalies were originally computed from a climatological baseline of 1951–1980, but are compared to the mean of the five previous years of each winter to be consistent with the model anomalies. The results are not dependent on the climatological period used.

To quantify changes to the Northern Hemisphere wintertime circulation, we compute the AO index as defined by the Climate Prediction Center (2020). The AO loading pattern is calculated as the first empirical orthogonal function (EOF) of sea level pressure anomalies from 20°N to 90°N for all months and all available years in each model. For WACCM4, a 60-year control run is used to calculate the loading pattern. The loading pattern is projected onto the first EOF of sea level pressure anomalies after the soot injections and volcanic eruptions, focusing on the DJF after the injection or eruption. The NAO is computed in the same way as the AO, but the area of interest for the EOF is restricted to between 90°W and 40°W. The NAO is a superior metric for quantifying the circulation response that leads to Eurasian winter warming (Ambaum et al., 2001).

3. Results

3.1. Surface Temperature Response

Following both the 1982 El Chichón and 1991 Pinatubo volcanic eruptions, anomalously warm surface temperatures were observed across North America and Eurasia during the first DJF after the eruptions (Figures 1b and 1c). The ensemble mean of surface temperature anomalies as simulated by the CESM-LE (Figures 1e and 1f) shows little resemblance to this pattern, and instead exhibits some warming in more northerly regions of the Arctic and Scandinavia, potentially from downwelling longwave radiation from the warm sulfate aerosol layer. The mean CESM-LE shows a very weak El Niño, which is not statistically significant. The ensemble mean of the AMIP-TOGA simulations, however, shows a compelling winter warming signal in the DJF after El Chichón over both North America and Eurasia (Figure 1h), and after Pinatubo the consistency in the warming signal over Eurasia is similar (Figure 1i). The winter warming pattern is also present in 9 out of 10 ensemble members after the El Chichón eruption. This indicates that when the model used in the CESM-LE is forced with observed tropical SSTs (including an El Niño event for each volcanic eruption), the modeled high-latitude temperature response is closer to the high-latitude winter warming response that is observed. Of course, there are some differences, since the real world only has one realization, and the observations are being compared to averages of multiple ensembles. The observed temperature pattern following the 1963 Agung eruption is less consistent with a high latitude winter warming pattern,

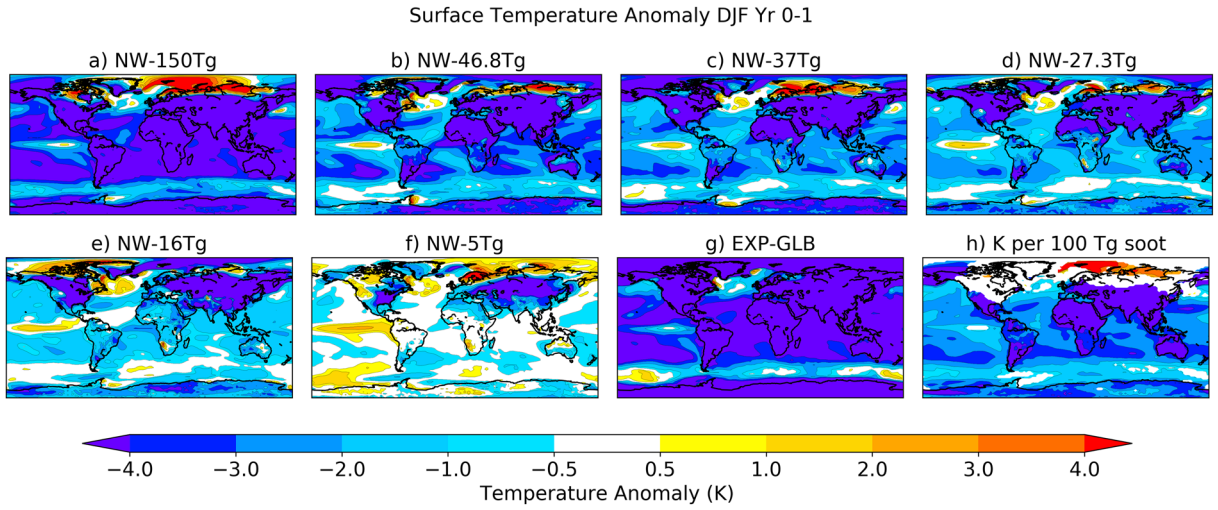

Figure 2. Whole Atmosphere Community Climate Model version 4 (WACCM4) (a–f) December-January-February (DJF) Year 0–1 surface air temperature anomaly (K) with respect to a 60-year control climatology for all six nuclear war scenarios and (g) EXP-GLB (case with NW-150 Tg cooling but no aerosol heating). (h) Linear regression of surface temperature anomaly per 100 Tg of soot injection during the first DJF after all six nuclear war scenarios.

as seen in Figure 1a. However, winter warming is simulated during DJF 1963–1964 in AMIP-TOGA (Figure 1g), which has prescribed tropical SSTs.

During all winters considered, warm equatorial Pacific SSTs were observed, which are included in AMIP-TOGA. This implies a role for warm equatorial Pacific SSTs, in combination with the stratospheric forcing from the large volcanic eruptions, in the winter warming response. AMIP-GOGA (Figures 1j–1l) exhibits very similar temperature patterns, indicating that it is tropical SSTs and not high-latitude ones that are needed for winter warming. The AMIP-GOGA results are therefore combined with AMIP-TOGA hereafter to provide 20 ensemble members in total for what will simply be referred to as the AMIP simulations.

In nuclear war simulations using WACCM4, we are able to explore how a far stronger and more vertically distributed aerosol forcing, which lasts for nearly a decade, affects the Northern Hemisphere wintertime circulation. Winter warming in the first year after stratospheric soot aerosol injection is mostly absent across North America, but is present in northern Eurasia for five out of six of the nuclear war simulations using WACCM4 (Figure 2). The surface temperature anomaly response per 100 Tg of soot is shown in Figure 2g, indicating a weak relationship between the amount of soot and the temperature response except for northern parts of Eurasia. A linear increase in the warming response is complicated by the intense global cooling, especially during summer, also associated with a soot injection, which mitigates warm air advection over Eurasia by cooling the areas upstream. In the second year after the soot injection, there is even less consistent winter warming, and then in years 3–10 cooling is dominant across much of the Northern Hemisphere. Volcanic eruptions do not produce the intense cooling that soot injections do, complicating a comparison between the two. The spatial distribution of the warming pattern in the nuclear war simulations is shifted poleward from the typical AO pattern, as well as what is seen following observed volcanic eruptions.

We performed an additional experiment with WACCM4, hereafter EXP-GLB, where the albedo of the surface is increased to mimic the reduction in shortwave radiation by the aerosols in NW-150 Tg, while the impact of aerosol heating is removed. The increase in the albedo averaged over the first six months of the simulation (15 May–15 November) is shown in Figure 3a. The surface temperature response for EXP-GLB (Figure 2g) shows minimal Eurasian warming due to a weaker circulation response. Because the surface temperature response can be masked by global cooling or shifted poleward with higher levels of soot, to understand the full breadth of the circulation response, we quantify changes to the SPV, AO, and NAO.

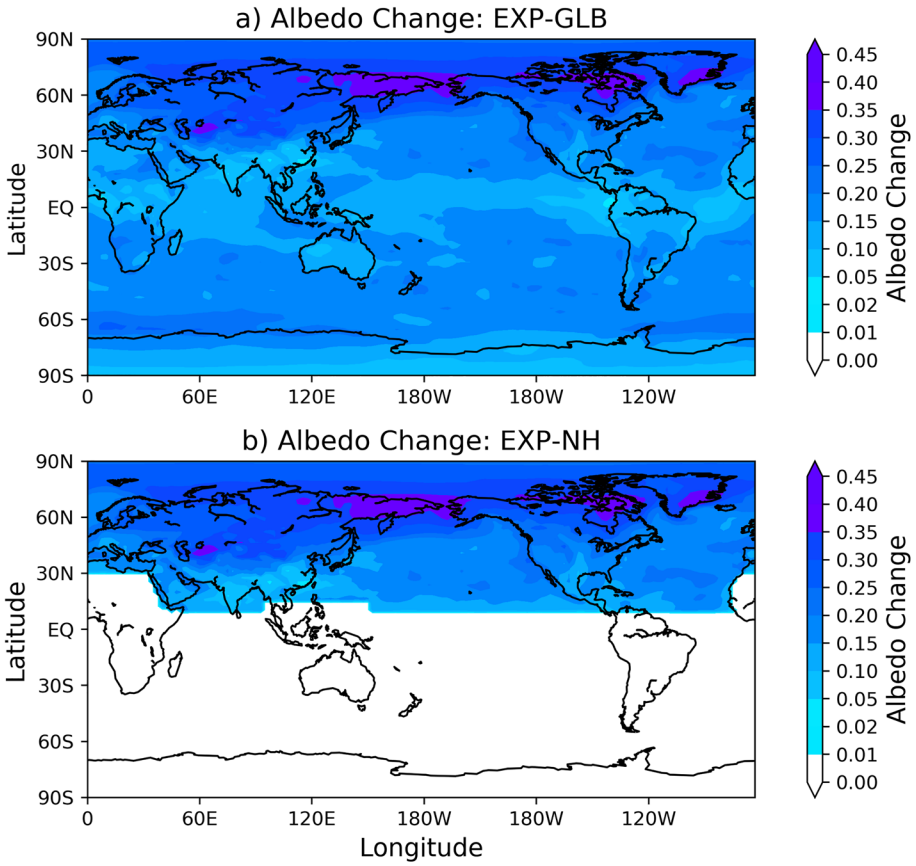

Figure 3. Change in albedo to mimic cooling from NW-150 Tg, averaged over the first 6 months, for experiments where aerosol heating is removed: (a) EXP-GLB and (b) EXP-NH.

3.2. Zonal Mean Stratospheric Polar Vortex Response

In the first winter after the 1982 El Chichón and 1991 Mt Pinatubo eruptions, in response to heating of stratospheric sulfate aerosols, a strengthened SPV was both observed and is simulated using models with a well-resolved stratosphere (Bittner et al., 2016; Polvani et al., 2019). The zonal mean wind acceleration attributed directly to the effect of the aerosols is often cited to be relatively weak, quantified as ~3–4 m s^{-1} at 10 hPa and 60°N during the winter of 1991–1992 in climate model ensembles (Bittner et al., 2016). In the ensemble mean of the CESM-LE, the zonal wind anomaly at 10 hPa and 60°N during this same time period is closer to 6 m s^{-1} following the three volcanic eruptions studied here. Figure 4a shows the zonal mean zonal wind anomaly profile at 60°N during DJF 1963–1964, DJF 1982–1983, and DJF 1991–1992, the first winters following the three largest volcanic eruptions of the twentieth century in the CESM-LE (42 ensembles) and combined AMIP-TOGA and AMIP-GOGA (20 ensembles total) simulations. The light and dark gray shading represents DJF climatology for the AMIP and CESM-LE simulations, respectively. The climatological bounds used to indicate natural variability are ±2 standard deviations of the zonal mean winds for the ensemble average of all winters between 1920 and 2000, but excluding winters immediately following a volcanic eruption. Both ensemble means show an acceleration of the SPV after all eruptions, but the strongest response is after the Pinatubo eruption (DJF 1991–1992), which is consistent with its larger initial sulfate aerosol loading (17 Tg SO_2). To quantify the contribution of the heating of the volcanic aerosols toward the strengthening of the meridional temperature gradient in the stratosphere, the difference between the solar heating rate (units of K day^{-1}) of the midlatitudes (30–60°N) and the polar regions (60–90°N) is calculated for the first winter after each eruption and shown in Figure 4b. This quantity represents differential heating by the aerosols in the midlatitudes and subtropics compared to the polar regions, where a positive value indicates the midlatitudes are heating more quickly than the polar regions. In much of the stratosphere, differences in differential heating explain the zonal mean zonal wind response differences, but there are

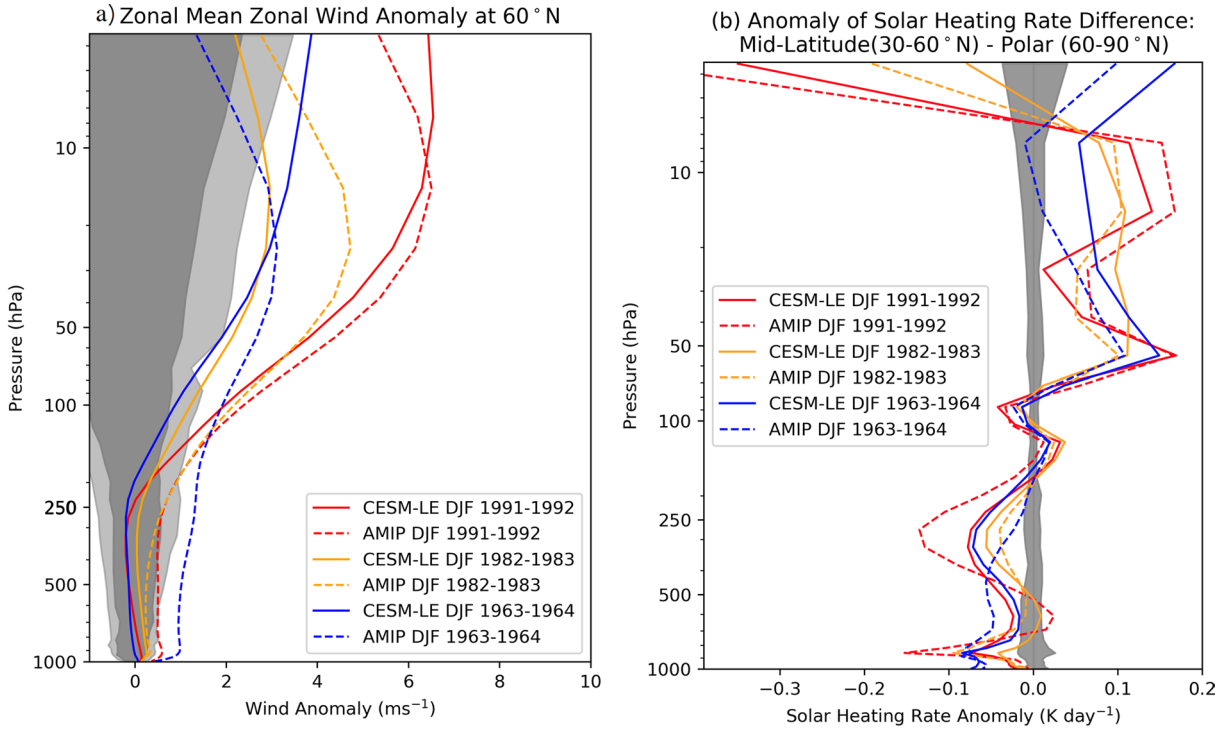

Figure 4. Zonal mean zonal wind anomaly (with respect to 1920–2000) profiles at 60°N during the first December-January-February (DJF) after volcanic eruptions in Community Earth System Model-Large Ensemble (CESM-LE) and Atmospheric Model Intercomparison Project (AMIP) (Tropical Ocean Global Atmosphere [TOGA] and Global Ocean Global Atmosphere [GOGA] combined). The light and dark gray shading represents DJF climatology for the AMIP and CESM-LE simulations, respectively. (b) The anomalous difference in the solar heating rate (K day^{-1}) for mid-latitudes (30–60°N) minus polar regions (60–90°N) during DJF as a function of height. The climatological bounds used to indicate natural variability are ±2 standard deviations of each variable for the ensemble average of all winters between 1920 and 2000.

discrepancies. The AMIP ensembles simulate a stronger SPV after the 1982 El Chichón eruption compared to CESM-LE, which is not indicated by their heating profiles. Notably, the 1982–1983 El Niño was much larger than the ones after the other two eruptions, a feature included in AMIP but not CESM-LE. The zonal wind anomaly at 60°N is also positive throughout the atmospheric column in AMIP, but not CESM-LE, showing stronger stratosphere-troposphere coupling in the AMIP runs that combine stratospheric and El Niño forcing. The mechanism for this is unclear, as previous work has suggested that El Niños are associated with negative AO and NAO indices, not positive ones (Oehrlein et al., 2019).

After the 1991 Pinatubo eruption, the AMIP ensembles also simulate a more positive zonal wind response throughout the column, up until 10 hPa, at which point the CESM-LE simulates a stronger SPV. Overall, the zonal wind response in the troposphere is more strongly correlated to the stratospheric response in AMIP compared to CESM-LE. This suggests that in the AMIP ensembles, despite a weaker acceleration of the SPV, it couples more strongly to the troposphere, which enables a surface temperature response closer to the observed temperature response (Eurasian winter warming) compared to the CESM-LE simulations (Figure 1). Next, we utilize the nuclear war simulations to further understand the mechanisms for the acceleration of the SPV due to aerosol heating and its coupling to the troposphere to produce the surface response.

In contrast to after volcanic eruptions, an acceleration of the SPV greater than 30 m s^{-1} is simulated in WACCM4 in even the smallest 5 Tg soot case. The forced Northern Hemisphere circulation response to soot injection in WACCM4 is characterized by a significant shift in the wintertime SPV on a decadal timescale, which coincides with an increase in the stratospheric meridional temperature gradient that is an order of magnitude larger than after volcanic eruptions. The mean response of the zonal mean zonal wind anomaly at 60°N is anomalously westerly throughout the stratosphere and troposphere for all soot injections during the first two winters (DJF), as indicated by Figure 5. A statistically significant enhancement of the decadal mean zonal mean zonal winds is present for all soot injections greater than 5 Tg and there is a linear

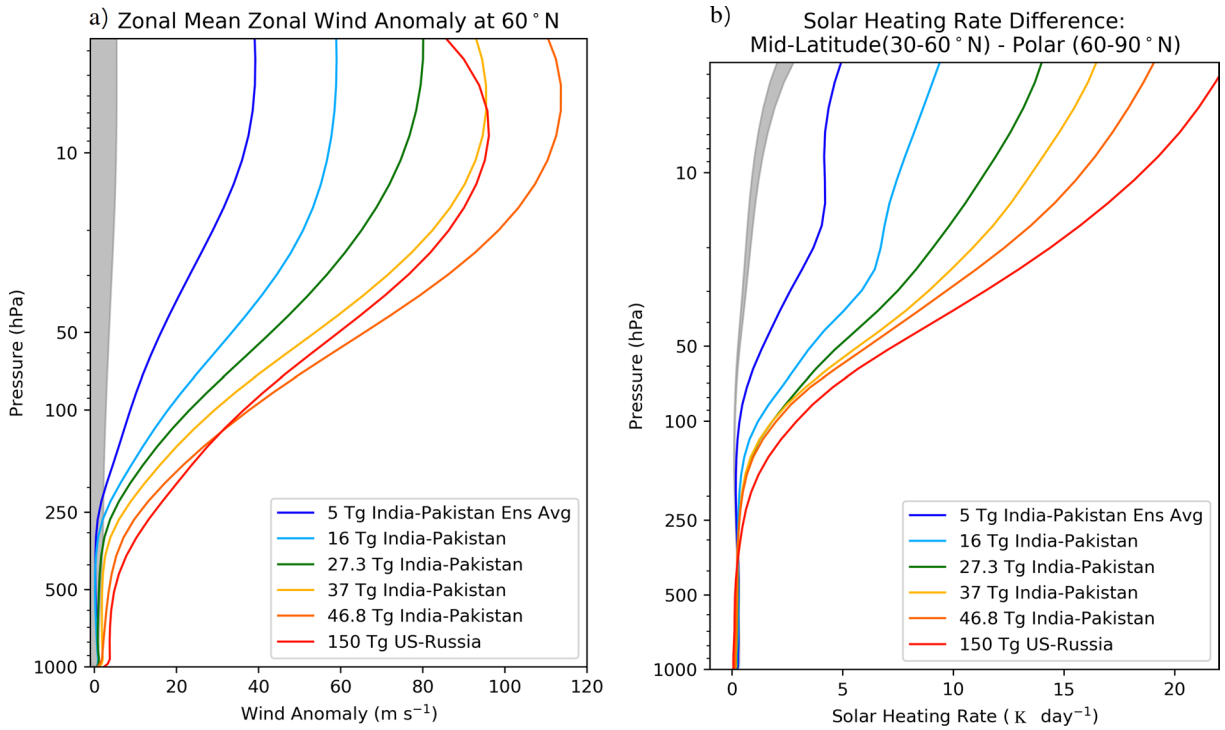

Figure 5. (a) Zonal mean zonal wind anomaly (m s^{-1}) with respect to control climatology at 60°N averaged during the first two December-January-February (DJF)s after six nuclear war scenarios. (b) The difference in the solar heating rate (K day^{-1}) for midlatitudes (30–60°N) minus polar regions (60–90°N) during DJF at 60°N as a function of height and soot injection. Gray shading represents ±2 standard deviations for each variable in the model DJF control climatology.

enhancement of the wind anomaly as a function of initial soot mass. To quantify the contribution of the highly absorptive soot aerosols toward the strengthening of the meridional temperature gradient in the stratosphere, we replicate Figure 4b for the soot injection cases, calculating the difference between the solar heating rate (units of K day^{-1}) of the midlatitudes (30–60°N) and the polar regions (60–90°N) for the first two winters. The extremely absorptive nature of the soot aerosols leads to tropical stratospheric temperature anomalies greater than 100 K for the first few years across the soot injection simulations, far greater and at higher altitudes than temperature anomalies observed after volcanic eruptions with sulfate aerosols (Figure 5b). The enhanced meridional temperature gradient is almost entirely driven by the aerosol heating and is then associated with a westerly acceleration of the zonal mean zonal winds. In most of the nuclear war simulations, the acceleration of the winds is highly correlated with changes in the meridional temperature gradient, although NW-150 Tg has weaker stratospheric winds compared to NW-46.8 Tg, despite a stronger solar heating gradient in NW-150 Tg. However, both cases exhibit very extreme SPV anomalies of greater than 80 m s^{-1}.

3.3. Mechanisms for Zonal Mean Stratospheric Polar Vortex Response

A simple linear regression of zonal mean zonal winds (units of m s^{-1}) at 50 hPa and averaged over 50–70°N, using the meridional temperature difference between the midlatitudes (30–60°N) minus the polar regions (60–90°N) at 50 hPa ($\Delta T_{50\,\mathrm{hPa}}$, units of K) as a predictor, reveals the physical connection between the temperature and winds, providing an estimate of the westerly acceleration of the SPV that can be explained by the aerosol heating, as shown for NW-150 Tg in Figure 6. The relationship between these variables in the control run is used to train this regression model, and we assume a linear relationship exists but acknowledge this may not be the case for larger levels of forcing. The acceleration of the SPV via aerosol heating and the propagation of this signal down toward the surface are referred to here as the stratospheric mechanism. In the first few years after the 150 Tg soot injection, changes in $\Delta T_{50\,\mathrm{hPa}}$ are able to explain ~70% of the zonal mean zonal wind anomaly during DJF, but this becomes smaller each subsequent DJF between years 3 and 10. For the other soot injection cases, a similar reduction in the proportion of SPV strengthening explained

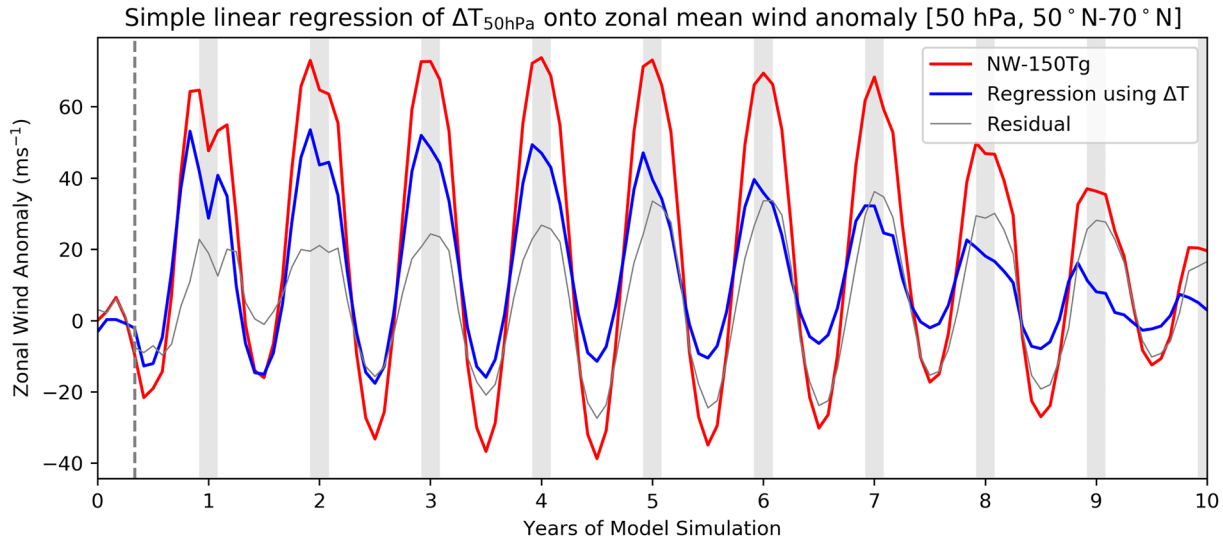

Figure 6. Linear regression of zonal mean zonal wind anomaly (m s^{-1}) at 50 hPa and averaged between 50°N and 70°N using the meridional temperature difference between 50°N and 70°N at 50 hPa ($\Delta T_{50\,hPa}$, units of K) as a predictor. Vertical dashed line is the time of injection of soot into the upper troposphere.

by aerosol heating through time is also observed. However, there is also an inverse relationship between initial soot loading and the correlation between aerosol heating and SPV strengthening for the first three winters after injection. For example, during the first winter of the 27.3 Tg case, the regression of the SPV anomaly using $\Delta T_{50\,hPa}$ as a predictor explains 90% of the SPV anomaly, compared to 70% for the 150 Tg case. As soot is increased, aerosol heating explains less of the SPV anomaly as global surface temperatures plummet from reduced sunlight. Two possible factors could explain this discrepancy. The first is that this may be evidence of a potential tropospheric mechanism in these simulations, in which global surface cooling can contribute to SPV strengthening. Thus, the regressed zonal winds using $\Delta T_{50\,hPa}$ are underestimated in simulations where the tropospheric mechanism plays a larger role. The second, is that these discrepancies may arise due to nonlinearities in the relationship between the strength of the SPV and the meridional temperature gradient. To settle this, later we will conduct additional experiments to test for the tropospheric mechanism.

The hypothetical tropospheric mechanism for acceleration of the SPV suggests surface cooling can reduce the total vertically and poleward propagating wave flux that enters the polar stratosphere. To explore this potential mechanism, we examine the vertical component of the zonally averaged Eliassen-Palm (E-P) flux during the first few winters after the soot injections, consistent with the work of Stenchikov et al. (2002) and using equation 2.1 from Andrews et al. (1983). Consistent with $\Delta T_{50\,hPa}$ in NW-150 Tg explaining the smallest proportion of SPV strengthening compared to the other soot injection cases, NW-150 Tg also exhibits the greatest reduction in global mean surface temperatures and vertical E-P flux in the mid-latitude upper troposphere. Generally, greater initial soot loading and more negative global surface temperature anomalies are associated with reduced vertical E-P flux, as shown in Figure 7. To confirm the role of surface cooling on the SPV anomaly, we conducted an additional simulation using WACCM4 where aerosol heating is removed, but the reduction in insolation is applied via an increase in albedo at the surface (EXP-GLB). The albedo modification is designed to mimic reduced shortwave radiation as a result of the aerosols in NW-150 Tg, the largest forcing case (Figure 3). Figure 7 includes this experiment, EXP-GLB, and shows a minor reduction in vertically propagating E-P flux. Although it is small, the reduction in E-P flux into the polar stratosphere appears to have a detectable contribution toward the circulation response in the 150 Tg case during the first two winters. Figure 7 shows the change in the zonal mean zonal winds at 50 hPa for all latitudes during the first DJF across all soot injection simulations, including EXP-GLB. The SPV strengthening in EXP-GLB is just larger than the two standard deviation envelope we have used to define natural variability, but explains only 15% of the total response for the largest 150 Tg case, and likely less than 15% for the smaller soot injections.

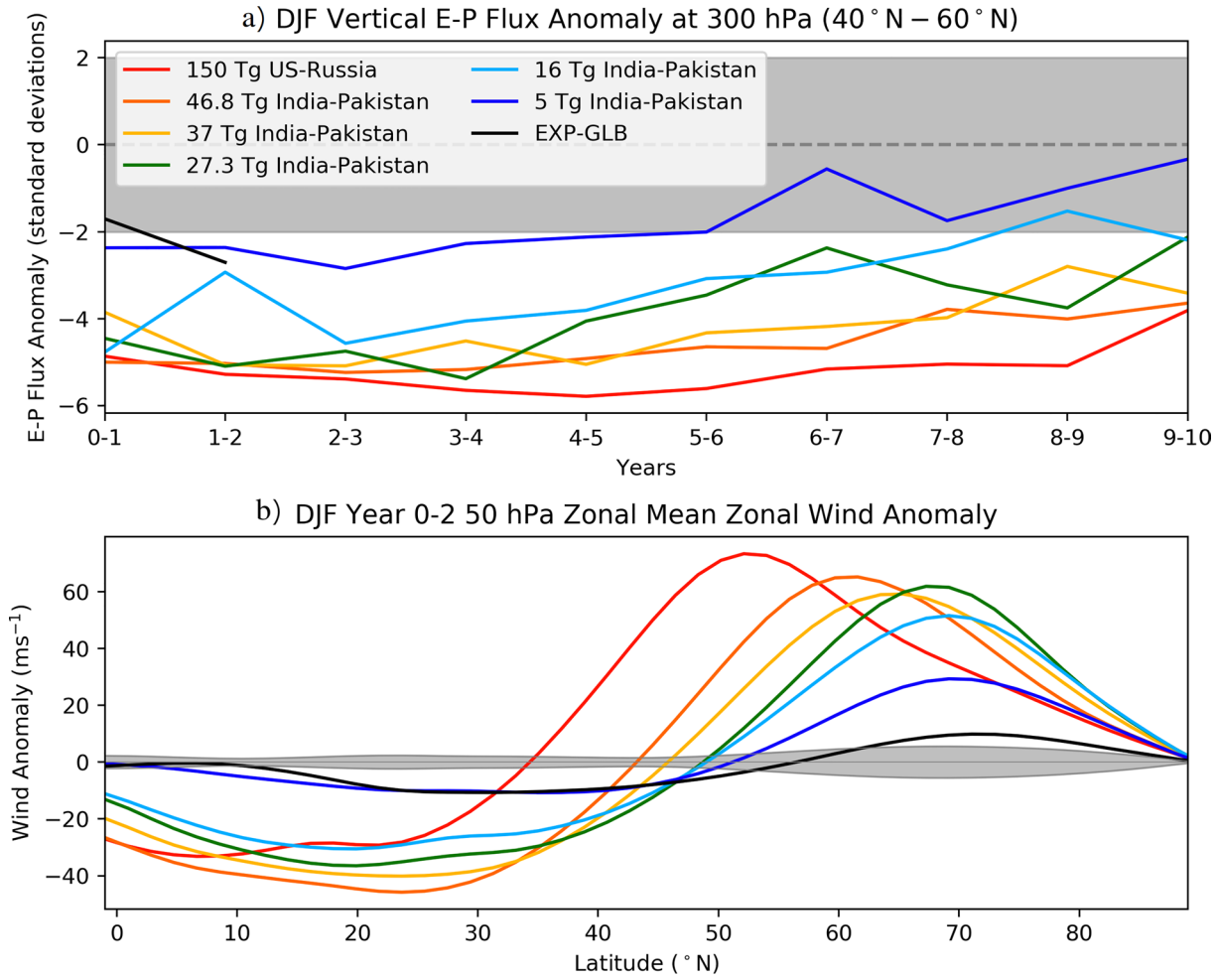

Figure 7. (a) Vertical component of the zonally averaged Eliassen-Palm (E-P) flux anomaly (standard deviations from the control mean) at 300 hPa and averaged for 40°N–60°N during December-January-February (DJF) in six nuclear war simulations, including the EXP-GLB sensitivity test. (b) Zonal mean zonal winds at 50 hPa as a function of latitude for all six nuclear war simulations, including the EXP-GLB sensitivity test. Gray shading represents ±2 standard deviations from the control mean climatology.

A weakly positive NAO is also simulated during the first DJF after the global albedo perturbation is applied in EXP-GLB, showing that this perturbation to the SPV is coupled to the troposphere in the North Atlantic without aerosol heating. However, this relatively small change for such a large perturbation (5 K global surface cooling in one year) does not support a major role for the tropospheric mechanism in accelerating the SPV after Pinatubo-sized volcanic eruptions, which produced far weaker surface cooling and negligible, or even positive changes to vertically propagating E-P Flux (Graf et al., 2007). We note that the AMIP simulations, with a stronger zonal mean zonal wind response than the CESM-LE at altitudes below 10 hPa, exhibit a statistically significant E-P flux divergence anomaly in the high latitude stratosphere during DJF 1991–1992 and 1982–1983 (Figure 8), despite the concurrent El Niño response. Thus, changes to E-P flux can contribute to the zonal mean zonal wind response, but the signal is weaker than the aerosol heating signal with a Pinatubo-sized volcanic eruption or smaller. We must also note that the reduction in E-P flux in the soot injection simulations is not solely a reflection of the tropospheric mechanism for cases with aerosol heating. Stratospheric aerosol heating and the associated meridional temperature gradient are actually necessary for a significant reduction in E-P flux, as the subsequent acceleration of the SPV tends to reflect vertically propagating waves back toward the surface, which is realized as a reduction in vertical E-P flux. Thus, the effect of surface cooling on E-P flux is rather small and is only identified when extremely large surface temperature perturbations are applied, at which point, anomalous winter warming can be masked by large-scale cooling. The only unresolved question is if reduced equatorial convection or reduced mid-latitude

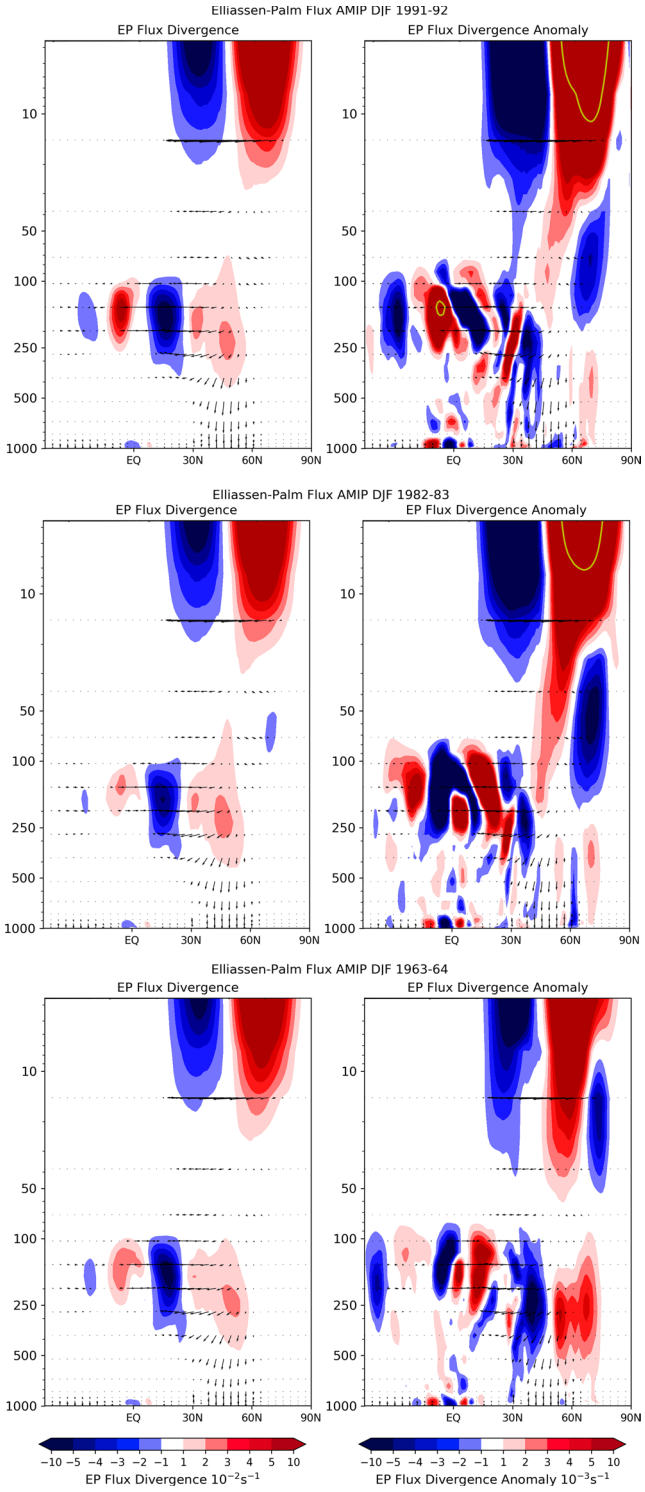

Figure 8. Atmospheric Model Intercomparison Project-Tropical Ocean Global Atmosphere (AMIP-TOGA) and AMIP-Global Ocean Global Atmosphere (GOGA) combined ensemble mean of Eliassen-Palm Flux Divergence (left, contours, 10^{-2} s^{-1}), the vertical and meridional components of the Eliassen-Palm Flux (vectors), and anomaly of the Eliassen-Palm Flux divergence (right contours, 10^{-3} s^{-1}) for (top) December-January-February (DJF) 1991–1992, (middle) DJF 1982–1983, and (bottom) DJF 1963–1964. Yellow contours indicate where anomalies are beyond a two standard deviation threshold compared to an ensemble mean climatology.

baroclinity is causing the reduction in E-P flux. To understand this, we conducted an additional simulation identical to EXP-GLB but with cooling only applied north of 15°N (see Figure 3b), hereafter EXP-NH. In EXP-NH, equatorial convection is not reduced as much and there is no significant reduction in E-P flux simulated, along with no observed SPV acceleration. We can conclude from this that the reduced equatorial convection is driving changes in E-P flux, in contrast with the findings of Stenchikov et al. (2002). Next, we evaluate the surface AO/NAO response to address the additional complication in characterizing how the acceleration of the SPV is then coupled to the troposphere.

3.4. Arctic Oscillation/North Atlantic Oscillation Response

Extreme SPV states typically couple to the troposphere and can have significant impacts on midlatitude weather. After volcanic eruptions, the forced signal of a subtle acceleration of the SPV contributes to a positive mode of both the AO and NAO at the surface during the first winter after eruption, but large ensembles are required to show this signal, as demonstrated by Bittner et al. (2016). In the CESM-LE and AMIP simulations we examined here, there is a larger acceleration of the SPV compared to the model (MPI-ESM-LR) used by Bittner et al. (2016). In AMIP (20 ensemble members) and the CESM-LE (42 ensemble members), the mean AO and NAO response is weakly positive. To assess the statistical significance of the response, the probability density function (PDF) is calculated for the AO/NAO during winters after volcanic eruptions (DJF 1963–1964, DJF 1982–1983, DJF 1991–1992) and compared to the PDF for all other winters. The Kolmogorov-Smirnov test is used to determine if there is a significant shift in the PDF between the volcanic and non-volcanic winters for all of the ensembles, where a p value less than 0.05 is deemed to be significant. Figure 9 shows the PDF for the AO and NAO for the average of DJF 1982–1983 and DJF 1991–1992 compared to all other winters in both the CESM-LE and AMIP ensemble mean response, with the p value corresponding to the forced response indicated on each graph. DJF 1963–1964 is not shown because there is no significant surface AO/NAO response for CESM-LE or AMIP.

For the CESM-LE, there is no significant shift in the PDF of the AO or NAO for DJF 1982–1983 or DJF 1991-1992 separately, or when combined, which is shown in Figure 9. In contrast, the AMIP results show a significant positive shift in the AO ($p = 0.003$) and NAO ($p < 0.001$) for the combined DJF 1982–1983 and DJF 1991–1992 period. The shift in the NAO is more significant and occurs for both DJF 1982–1983 and DJF 1991-1992 separately in AMIP. After soot injections associated with a potential nuclear war, there is a far less ambiguous positive shift in the AO/NAO due to the more robust acceleration of the SPV over a longer timescale. Figures 9c and 9f show the PDF of the AO and NAO for the 10 winters after the six soot injections. A longer time period is selected because of the lack of ensembles, but in the decade after the soot injections, there is a statistically significant shift in the AO/NAO for all cases, with the exception of the NAO in NW-46.8 Tg, an outlier. A significant NAO response was not identified in the mean of 42 ensemble members for the two eruptions in the CESM-LE, so it is not entirely surprising that a significant signal could not always be detected in the 10 winters after soot injections. Nevertheless, these results indicate strong coupling between the stratosphere and troposphere after soot injections in WACCM4, while volcanic eruptions in the CESM-LE and AMIP do not facilitate as strong of a surface response to SPV acceleration.

The WACCM4 soot injection simulations show the strongest coupling between the stratosphere and lower troposphere, followed by AMIP-TOGA, AMIP-GOGA, then CESM-LE. Greater coupling in soot injections is best explained by the extreme acceleration of the SPV, which is more likely to couple to the troposphere and more likely to produce a positive NAO. The greater vertical lofting of the soot aerosols may also play a small role in promoting stronger coupling in the nuclear war simulations compared to volcanic eruptions, but the zonal mean zonal wind response with height is very similar, despite strong aerosol heating at higher altitudes. The mechanism for stronger coupling in AMIP-TOGA, when observed SSTs are prescribed in tropical regions, should be explored further. The observed tropical SSTs include a strong El Niño for DJF 1982–1983, a moderate one for DJF 1991–1992, and a weak one for DJF 1963–1964, and in each ensemble member (not shown) and the mean of the AMIP runs, the model simulates winter warming (Figure 1). The same model (CESM-LE) does not produce a statistically significant El Niño signal following the large volcanic eruptions (Figure 1, second row), but if one is specified, then that model does produce a positive NAO and winter warming. This suggests that there is a role for El Niño through a tropospheric mechanism. Graf et al. (2014) used observations to hint that the high latitude response to large volcanic eruptions could be modulated by

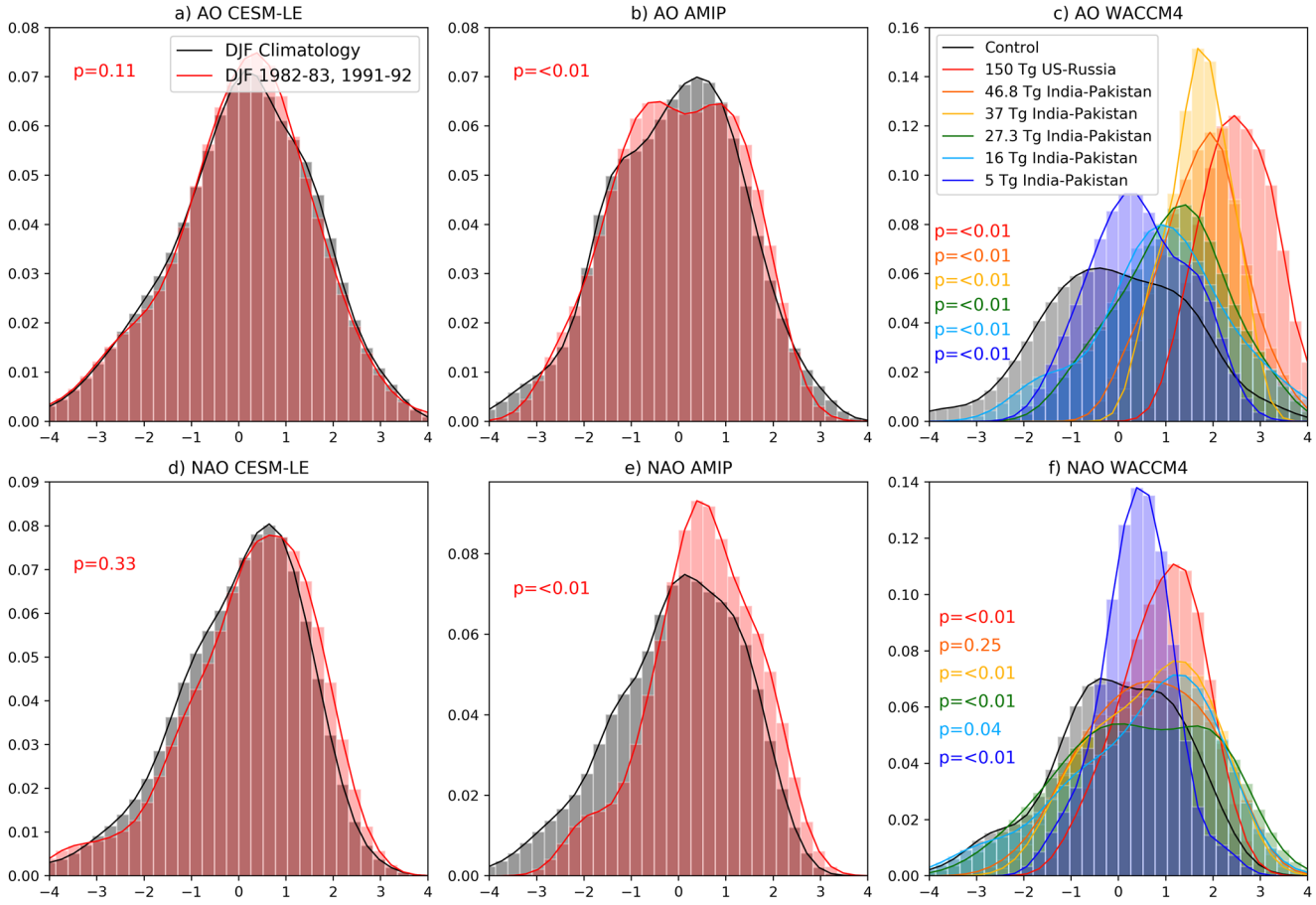

Figure 9. Probability density function (PDF) of the Arctic Oscillation (AO) for December-January-February (DJF) 1982–1983 and 1991–1992 compared to DJF climatology for (a) Community Earth System Model-Large Ensemble (CESM-LE), (b) Atmospheric Model Intercomparison Project (AMIP). The PDF for 10 winters (DJF) after nuclear war simulations compared to control climatology is shown in (c). (d–f) Shows the same as (a–c) but for the North Atlantic Oscillation (NAO).

tropical SSTs because the resulting patterns of tropical convection and atmospheric heating stimulate wave trains that propagate into higher latitudes. But they found there were too few examples of large volcanic eruptions with good data to make strong conclusions. Ding et al. (2017) examined the effects of La Niña on European winter temperatures, and found the opposite of the pattern we found, suggesting that El Niños would warm Europe in the winter. Oehrlein et al. (2019) showed that El Niños typically are associated with a negative mode of the NAO in the troposphere, but that is in the absence of strong stratospheric forcing. A tropospheric mechanism connecting equatorial Pacific warming and negative NAO-like variability in the North Atlantic was also proposed by Mezzina et al. (2020), in contrast to the positive NAO in the AMIP simulations. In the CESM-LE simulations, there is no indication that the relationship between Niño3.4 SST anomalies and the NAO is any different during volcanic winters compared to non-volcanic winters, also in contrast to AMIP.

4. Conclusions

Simulations of soot injections in a coupled climate model show that aerosol heating is the primary contributor toward the acceleration of the SPV. This response couples to the surface quite easily and generates a winter warming response that is poleward of the response observed after volcanic eruptions, due to the poleward movement of the polar jet. The potential tropospheric mechanism for the acceleration of the vortex is a contributor as well, but mostly for the largest soot injection cases. In the most extreme case, NW-150 Tg, this mechanism statistically explains at most 15% of the response. In the AMIP simulations of

volcanic eruptions, a statistically significant change in E-P flux divergence occurs in a small part of the high latitude stratosphere, but the aerosol heating signal is larger after a Pinatubo-sized volcanic eruption. Given this, one can infer that in a smaller forcing scenario (i.e., a volcanic eruption), the tropospheric mechanism alone would not be able to explain as much of the changes to the SPV. However, the ratio of aerosol heating to surface cooling is larger in the nuclear war simulations compared to the volcanic eruptions, leaving open the possibility that the tropospheric mechanism may hold more importance in volcanic eruptions, at least relative to the nuclear war simulations.

An analysis of volcanic eruptions in the CESM-LE and AMIP simulations shows a weak but statistically significant acceleration of the SPV, and a significant shift in the NAO and AO when the winters of 1982–1983 and 1991–1992 are considered together with specified SSTs matching the observed climate change in those winters. The lack of a winter warming signal in the CESM-LE, where SSTs are internally generated, suggests that the inability of the model to generate the observed El Niño prevents it from simulating the winter warming, because stratospheric and surface forcing are both required for a winter warming response with this level of stratospheric forcing. However, differences in the strength of troposphere-stratosphere coupling between the two ensemble simulations show that despite a more robust SPV response, there are considerable uncertainties regarding the surface circulation and subsequent temperature response for Pinatubo-sized volcanic eruptions. We find a positive NAO response at the surface following volcanic eruptions with stratospheric heating, but El Niño-like warming of the equatorial Pacific increases the probability of the positive NAO response and winter warming. It is possible that the observed winter warming following the 1982 El Chichón and 1991 Pinatubo eruptions occurred by chance, but the observed stratospheric heating and El Niño are two common factors between the events. Our results suggest that with an El Niño and a large volcanic eruption, the combined tropospheric and stratospheric forcings work together to produce winter warming, but if there are different sea surface temperature patterns, they can work to prevent winter warming. Since there is evidence that indeed volcanic eruptions increase the probability of an El Niño in the next winter (e.g., Khodri et al., 2017), when climate models get to the point that they can robustly simulate this El Niño response, we suggest that they will also simulate winter warming. However, more work is needed to understand the exact mechanisms that explain how the presence of an El Niño combined with stratospheric forcing from a large volcanic eruption produces a positive NAO.

Data Availability Statement

The CESM-LE data set has been made available at NCAR's Climate Data Gateway with instructions can be found at http://www.cesm.ucar.edu/projects/community-projects/LENS/data-sets.html. AMIP-TOGA and AMIP-GOGA are available via NCAR's Climate Data Gateway as well, with instructions, at http://www.cesm.ucar.edu/working_groups/CVC/simulations/cam5-prescribed_sst.html. Postprocessed output from NW-150 Tg can be found at https://figshare.com/articles/dataset/WACCM4_150_Tg_US-Russia/7742735. Postprocessed output for the 5-46.8 Tg simulations can be found at: https://doi.org/10.6084/m9.figshare.14370785.v1.

Acknowledgments
This study is supported by the Open Philanthropy Project, NSF grant AGS-1430051, and a Faculty Fellowship for Alan Robock from the Cooperative Institute for Research in Environmental Sciences, University of Colorado, Boulder. The authors thank the National Center for Atmospheric Research, which is funded by NSF, in particular the Climate Variability and Change Working Group, for access to the large ensemble simulations analyzed here. They would like to thank Antara Banerjee, Lorenzo Polvani, Jennifer Kay, Hans Graf, and Georgiy Stenchikov for valuable suggestions, Lili Xia for helping with the large ensemble analysis, and Adam S. Phillips for conducting the AMIP simulations.

References

Ambaum, M. H. P., Hoskins, B. J., & Stephenson, D. B. (2001). Arctic oscillation or North Atlantic oscillation? *Journal of Climate*, *14*, 3495–3507. https://doi.org/10.1175/1520-0442(2001)014<3495:AOONAO>2.0.CO;2

Andrews, D. G., Mahlman, J. D., & Sinclair, R. W. (1983). Eliassen-Palm diagnostics of wave-mean flow interaction in the GFDL "SKYHI" general circulation model. *Journal of the Atmospheric Sciences*, *40*, 2768–2784. https://doi.org/10.1175/1520-0469(1983)040<2768:ETWATM>2.0.CO;2

Baldwin, M. P., & Dunkerton, T. J. (2001). Stratospheric harbingers of anomalous weather regimes. *Science*, *294*, 581–584. https://doi.org/10.1126/science.1063315

Banerjee, A., Butler, A. M., Polvani, L. M., Robock, A., Simpson, I. R., & Sun, L. (2021). Robust winter warming over Eurasia under stratospheric sulfate geoengineering: The role of stratospheric dynamics. *Atmospheric Chemistry and Physics*, *21*, 6985–6997. https://doi.org/10.5194/acp-21-6985-2021

Bardeen, C. G., Garcia, R. R., Toon, O. B., & Conley, A. J. (2017). On transient climate change at the Cretaceous–Paleogene boundary due to atmospheric soot injections. *Proceedings of the National Academy of Sciences*, *114*, E7415–E7424. https://doi.org/10.1073/pnas.1708980114

Bardeen, C. G., Toon, O. B., Jensen, E. J., Marsh, D. R., & Harvey, V. L. (2008). Numerical simulations of the three-dimensional distribution of meteoric dust in the mesosphere and upper stratosphere. *Journal of Geophysical Research*, *113*, D17202. https://doi.org/10.1029/2007JD009515

Bittner, M., Schmidt, H., Timmreck, C., & Sienz, F. (2016a). Using a large ensemble of simulations to assess the Northern Hemisphere stratospheric dynamical response to tropical volcanic eruptions and its uncertainty. *Geophysical Research Letters*, *43*, 9324–9332. https://doi.org/10.1002/2016GL070587

Bittner, M., Timmreck, C., Schmidt, H., Toohey, M., & Krüger, K. (2016b). The impact of wave-mean flow interaction on the Northern Hemisphere polar vortex after tropical volcanic eruptions. *Journal of Geophysical Research: Atmospheres*, *121*, 5281–5297. https://doi.org/10.1002/2015JD024603

Climate Prediction Center. (2020). *Arctic oscillation (AO)*. Retrieved from https://www.cpc.ncep.noaa.gov/products/precip/CWlink/daily_ao_index/ao.shtml

Coupe, J., Bardeen, C. G., Robock, A., & Toon, O. B. (2019). Nuclear winter responses to nuclear war between the United States and Russia in the whole Atmosphere Community Climate Model Version 4 and the Goddard Institute for Space Studies ModelE. *Journal of Geophysical Research: Atmospheres*, *124*, 8522–8543. https://doi.org/10.1029/2019JD030509

Coupe, J., Stevenson, S., Lovenduski, N. S., Rohr, T., Harrison, C. S., Robock, A., et al. (2021). Nuclear Niño response observed in simulations of nuclear war scenarios. *Communications Earth & Environment*, *2*, 1–11. https://doi.org/10.1038/s43247-020-00088-1

DallaSanta, K., Gerber, E. P., & Toohey, M. (2019). The circulation response to volcanic eruptions: The key roles of stratospheric warming and eddy interactions. *Journal of Climate*, *32*, 1101–1120. https://doi.org/10.1175/JCLI-D-18-0099.1

Deser, C., Simpson, I. R., McKinnon, K. A., & Phillips, A. S. (2017). The Northern Hemisphere extra-tropical atmospheric circulation response to ENSO: How well do we know it and how do we evaluate models accordingly? *Journal of Climate*, *30*, 5059–5082. https://doi.org/10.1175/JCLI-D-16-0844.1

Ding, S., Chen, W., Feng, J., & Graf, H.-F. (2017). Combined impacts of PDO and two types of La Niña on climate anomalies in Europe. *Journal of Climate*, *30*, 3253–3278. https://doi.org/10.1175/JCLI-D-16-0376.1

GISTEMP Team. (2020). *GISS surface temperature analysis (GISTEMP), version 4*. NASA Goddard Institute for Space Studies. Retrieved from https://data.giss.nasa.gov/gistemp

Graf, H.-F., Kirchner, I., Robock, A., & Schult, I. (1993). Pinatubo eruption winter climate effects: Model versus observations. *Climate Dynamics*, *9*, 81–93. https://doi.org/10.1007/BF00210011

Graf, H.-F., Li, Q., & Giorgetta, M. A. (2007). Volcanic effects on climate: Revisiting the mechanisms. *Atmospheric Chemistry and Physics*, *7*, 4503–4511. https://doi.org/10.5194/acp-7-4503-2007

Graf, H.-F., Zanchettin, D., Timmreck, C., & Bittner, M. (2014). Observational constraints on the tropospheric and near-surface winter signature of the Northern Hemisphere stratospheric polar vortex. *Climate Dynamics*, *43*, 3245–3266. https://doi.org/10.1007/s00382-014-2101-0

Jones, A., Haywood, J. M., Jones, A. C., Tilmes, S., Kravitz, B., & Robock, A. (2020). North Atlantic Oscillation response in GeoMIP experiments G6solar and G6sulfur: Why detailed modelling is needed for understanding regional implications of solar radiation management. *Atmospheric Chemistry and Physics*, *21*, 1287–1304. https://doi.org/10.5194/acp-2020-802

Kay, J. E., Deser, C., Phillips, A., Mai, A., Hannay, C., Strand, G., et al. (2015). The Community Earth System Model (CESM) Large Ensemble Project: A community resource for studying climate change in the presence of internal climate variability. *Bulletin of the American Meteorological Society*, *96*, 1333–1349. https://doi.org/10.1175/BAMS-D-13-00255.1

Khodri, M., Izumo, T., Vialard, J., Janicot, S., Cassou, C., Lengaigne, M., et al. (2017). Tropical explosive volcanic eruptions can trigger El Niño by cooling tropical Africa. *Nature Communications*, *8*, 778. https://doi.org/10.1038/s41467-017-00755-6

Lehner, F., Deser, C., Simpson, I. R., & Terray, L. (2018). Attributing the U.S. Southwest's recent shift into drier conditions. *Geophysical Research Letters*, *45*, 6251–6261. https://doi.org/10.1029/2018GL078312

Lenssen, N., Schmidt, G., Hansen, J., Menne, M., Persin, A., Ruedy, R., & Zyss, D. (2019). Improvements in the GISTEMP uncertainty model. *Journal of Geophysical Research Atmospheres*, *124*, 6307–6326. https://doi.org/10.1029/2018JD029522

Marsh, D. R., Mills, M. J., Kinnison, D. E., Lamarque, J.-F., Calvo, N., & Polvani, L. M. (2013). Climate change from 1850 to 2005 simulated in CESM1(WACCM). *Journal of Climate*, *26*, 7372–7391. https://doi.org/10.1175/JCLI-D-12-00558.1

Mezzina, B., García-Serrano, J., Bladé, I., & Kucharski, F. (2020). Dynamics of the ENSO teleconnection and NAO variability in the North Atlantic–European late winter. *Journal of Climate*, *33*, 907–923. https://doi.org/10.1175/jcli-d-19-0192.1

Oehrlein, J., Chiodo, G., & Polvani, L. M. (2019). Separating and quantifying the distinct impacts of El Niño and sudden stratospheric warmings on North Atlantic and Eurasian wintertime climate. *Atmospheric Science Letters*, *20*, e923. https://doi.org/10.1002/asl.923

Polvani, L. M., Banerjee, A., & Schmidt, A. (2019). Northern Hemisphere continental winter warming following the 1991 Mt. Pinatubo eruption: Reconciling models and observations. *Atmospheric Chemistry and Physics*, *19*, 6351–6366. https://doi.org/10.5194/acp-19-6351-2019

Robock, A., & Mao, J. (1992). Winter warming from large volcanic eruptions. *Geophysical Research Letters*, *19*, 2405–2408. https://doi.org/10.1029/92GL02627

Robock, A., Oman, L., & Stenchikov, G. L. (2007). Nuclear winter revisited with a modern climate model and current nuclear arsenals: Still catastrophic consequences. *Journal of Geophysical Research*, *112*, D13107. https://doi.org/10.1029/2006JD008235

Stenchikov, G., Robock, A., Ramaswamy, V., Schwarzkopf, M. D., Hamilton, K., & Ramachandran, S. (2002). Arctic Oscillation response to the 1991 Mount Pinatubo eruption: Effects of volcanic aerosols and ozone depletion. *Journal of Geophysical Research*, *107*, 4803. https://doi.org/10.1029/2002JD002090

Tilmes, S., Richter, J. H., Kravitz, B., MacMartin, D. G., Mills, M. J., Simpson, I. R., et al. (2018). CESM1(WACCM) stratospheric aerosol geoengineering large ensemble project. *Bulletin of the American Meteorological Society*, *99*, 2361–2371. https://doi.org/10.1175/BAMS-D-17-0267.1

Toohey, M., Krüger, K., Bittner, M., Timmreck, C., & Schmidt, H. (2014). The impact of volcanic aerosol on the Northern Hemisphere stratospheric polar vortex: Mechanisms and sensitivity to forcing structure. *Atmospheric Chemistry and Physics*, *14*, 13063–13079. https://doi.org/10.5194/acp-14-13063-2014

Toon, O. B., Bardeen, C. G., Robock, A., Xia, L., Kristensen, H., McKinzie, M., et al. (2019). Rapidly expanding nuclear arsenals in Pakistan and India portend regional and global catastrophe. *Science Advances*, *5*, eaay5478. https://doi.org/10.1126/sciadv.aay5478

Toon, O. B., Turco, R. P., Westphal, D., Malone, R., & Liu, M. (1988). A multidimensional model for aerosols: Description of computational analogs. *Journal of the Atmospheric Sciences*, *45*, 2123–2144. https://doi.org/10.1175/1520-0469(1988)045<2123:AMMFAD>2.0.CO;2

Zambri, B., & Robock, A. (2016). Winter warming and summer monsoon reduction after volcanic eruptions in Coupled Model Intercomparison Project 5 (CMIP5) simulations. *Geophysical Research Letters*, *43*, 10920–10928. https://doi.org/10.1002/2016GL070460